nature geoscience

Article

https://doi.org/10.1038/s41561-022-01087-x

Siberian carbon sink reduced by forest disturbances

In the format provided by the authors and unedited

Supporting Information

Table of content

Supplementary Text

Method of estimation of aboveground carbon stocks from CWD and live AGC

The net land-atmosphere carbon exchange results from the changes in live AGC (AGC_{live}, estimated by L-VOD), from changes in the litter and soil carbon pools and from a lagged CO_2 emission from decaying coarse woody debris (CWD). Ignoring the soil and fine litter changes, the total aboveground carbon stocks (AGC_{tot}) are defined here as the sum of AGC_{live} and total CWD carbon stocks ($CWDC_{tot}$), accounting for the net changes of live and dead aboveground carbon stocks in terrestrial ecosystems at temporal and spatial scales:

$$AGC_{tot} = AGC_{live} + CWDC_{tot} \quad (1)$$

Over the Siberian forests, CWD carbon stocks ($CWDC$) is mainly driven by the background mortality and forest disturbances (e.g., wildfire, windstorm and droughts). The carbon loss from $CWDC$ were determined using decomposition and consumption by fires[1]. This decomposition rate is low because of low temperatures and short growing seasons[2], relative to tropical forests. Stand-replacing fire is the main cause of natural tree die-off in Siberia[3,4], increasing $CWDC$ in some areas, but also consuming $CWDC$. Here, the CO_2 emission from CWD was assumed to be induced by decomposition (Section 1.1 below) and combustion by stand-replacing fire (Section 1.2 below). Thus, $CWDC_{tot}$ was computed as the sum of carbon stocks resulting from (1) mortality of trees caused by stand-replacing fire ($CWDC_{stand-replacing}$), (2) the initial accumulation for years before 2010 ($CWDC_{initial}$), and (3) the mortality of trees by annually background mortality ($CWDC_{background\ mortality}$), and expressed as:

$$CWDC_{tot} = CWDC_{stand-replacing} + CWDC_{initial} + CWDC_{background\ mortality} \quad (2)$$

In addition, accounting for the different climatic regions, separate calculations of the CWD carbon stocks were made for Western Siberia, East Siberia and Far East regions, of which three climatic regions including Northern taiga, Middle taiga and Southern Taiga were accounted, respectively (Fig. S17).

In Section 1.1 below, we gave the details of calculations of the $CWDC$ decomposition. Details of the calculations of $CWDC_{stand-replacing}$, $CWDC_{initial}$ and $CWDC_{background\ mortality}$ are given in Section 1.2.

1.1 Decomposition of CWD carbon stocks

Through decomposition, $CWDC$ is partly released to the atmosphere via heterotrophic respiration, partly transformed to fine litter and soil carbon pools via fragment litter, and partly leached to dissolved organic carbon. Since respiration comprises the majority of carbon loss during CWD decay[2], we assumed that the decay loss of $CWDC$ is directly emitted to the atmosphere as CO_2. The changes in carbon stocks of CWD over time were expressed using a first-order kinetics model[2] :

$$CWDC_t = CWDC_{t=0} \times e^{-kt} \qquad (3)$$

where $CWDC_t$ is the CWD carbon stocks at tth year, $CWDC_{t=0}$ is the initial value of CWDC at time $t = 0$, and k is the decomposition rate at which $CWDC$ decreases over time, listed in Table S3 based on plot-level studies.

1.2 Changes in CWDC by accounting for decomposition and combustion

We calculated changes of $CWDC$ from (1) the initial accumulation prior to 2010 ($CWDC_{initial}$), (2) mortality of trees caused by stand-replacing fire ($CWDC_{stand-replacing}$), and (3) mortality of trees by annual background mortality, e.g., self-thinning and other stand dynamic processes ($CWDC_{background\ mortality}$) .

Four parameters were used in the calculations:

$Ratio_{initial}$, the ratio of $CWDC_{initial}$ to AGC_{live} in 2010 ($AGC_{live,2010}$) was estimated based on plot-level studies (Table S4), which included the consequence of previous stand replacing fires, because all forests in Siberia experienced fire at some point in the past.

$Ratio_{AGC\_consumption}$, the ratio of AGC_{live} consumption during stand-replacing fire events (Table S5).

$Ratio_{CWD_{consumption}}$, assumed to be a constant, is the percentage of coarse woody

debris consumed during stand-replacing fire events (Table S6).

$Ratio_{background\ mortality}$, assumed to be a constant, is the ratio of annual background mortality to $AGC_{live,2010}$ (Table S7).

$Fraction_i$, the percentage of stand-replacing fire area within the SMOS-grid (25×25km) at year i. Annual stand-replacing fire area from 2010-2019 was provided by ref[5].

(1) Initial CWD carbon stocks ($CWDC_{initial}$)

The year 2010 was considered to be the initial year, and $CWDC_{initial}$ was defined as the total carbon stocks of CWD at the initial state, which has accumulated prior to 2010. Because $CWD_{initial}$ can not be measured over the whole study region, it was estimated from the ratio between CWDC at initial state and AGC_{live} in 2010 ($AGC_{live,2010}$) as:

$$CWDC_{initial} = AGC_{live,2010} \times Ratio_{initial} \quad (4)$$

Then, accounting for decomposition and combustion due to stand-replacing fires in subsequent years, $CWDC_{initial}$ in the following years can be calculated as:

***In 2011:*

$$CWDC_{initial,2011} = CWDC_{initial} \times e^{-k} \times \left(1 - Fraction_{2011} \times Ratio_{CWD_{consumption}}\right) \quad (5)$$

***In 2012:*

$$CWDC_{initial,2012} = CWDC_{initial} \times e^{-2k} \times \left(1 - Fraction_{2011} \times Ratio_{CWD_{consumption}}\right) \times \left(1 - Fraction_{2012} \times Ratio_{CWD_{consumption}}\right) \quad (6)$$

***In year n:*

$$CWDC_{initial,n} = CWDC_{initial} \times e^{-k\times(n-2010)} \times \prod_{i=2011}^{n} (1 - Fraction_i \times Ratio_{CWD_{consumption}}) \quad (7)$$

(2) CWD carbon stocks induced by stand-replacing fire ($CWDC_{stand-replacing}$)

Stand-replacing fires are defined in this study as fire events that lead to substantial tree mortality due to fire damage, immediately or during subsequent years after the fire[5]. Meanwhile, combustion during stand-replacing fires typically removes ca. 1% of AGC_{live} (Table S5) and 65% of the accumulated $CWDC_{stand-replacing}$ in previous years (Table S6). Thus, total $CWDC$ induced by stand-replacing fires at year n ($CWDC^{total}_{stand-replacing,n}$) included two components: (1) the increment of $CWDC$ formed by stand-replacing fires in year n, and (2) the accumulated $CWDC$ from previous years, including carbon losses caused by combustion and decomposition. Thus, the calculation of $CWDC^{total}_{stand-replacing,n}$ was described by:

***In 2011:*

The increment of $CWDC$ induced by stand-replacing fire in 2011:

$$CWDC_{stand-replacing,2011} = AGC_{live,2010} \times \left(1 - Ratio_{AGC_{consumption}}\right) \times Fraction_{2011} \quad (8)$$

where $AGC_{live,2010}$ is the AGC_{live} in year 2010.

Then, the total carbon stocks of CWD caused by stand-replacing fire in 2011 were expressed as:

$$CWDC^{total}_{stand-replacing,2011} = CWDC_{stand-replacing,2011} \quad (9)$$

***In 2012:*

a. The increment of $CWDC$ induced by stand-replacing fire in 2012:

$$CWDC_{stand-replacing,2012} = AGC_{live,2011} \times \left(1 - Ratio_{AGC_{consumption}}\right) \times Fraction_{2012} \quad (10)$$

b. $CWDC_{stand-replacing,2011}$ was decayed and consumed in 2012, expressed as:

$$CWDC^{2011}_{stand-replacing,2012} = CWDC_{stand-replacing,2011} \times e^{-k} \times \left(1 - Fraction_{2012} \times Ratio_{CWD_{consumption}}\right) \quad (11)$$

Then, the total carbon stocks of CWD caused by stand-replacing fires in 2012 were expressed as:

$$CWDC^{total}_{stand-replacing,2012} = CWDC_{stand-replacing,2012} + CWDC^{2011}_{stand-replacing,2012} \quad (12)$$

Thus,

****In year n :*

The total carbon stocks of CWD ($CWDC^{total}_{stand-replacing,n}$) caused by stand-replacing fires at $year\ n$ were expressed as:

$$CWDC^{total}_{stand-replacing,n} = CWDC_{stand-replacing,n} + CWDC^{total}_{stand-replacing,n-1} \times \left(1 - Fraction_n \times Ratio_{CWD_{consumption}}\right) \quad (13)$$

where $2013 \leq n \leq 2019$, $CWDC_{stand-replacing,n}$ in *year n* was calculated using the following expression:

$$CWDC_{stand-replacing,n} = AGC_{live,n-1} \times \left(1 - Ratio_{AGC_{consumption}}\right) \times Fraction_n \quad (14)$$

where $AGC_{live,n-1}$ is AGC_{live} at the year before fire.

(3) CWD carbon stocks produced by annual background mortality ($CWDC_{background\ mortality}$)

Similar to the calculation of $CWDC_{stand-replacing}$ above, total CWD carbon stocks induced by background mortality at $year\ n$ ($CWDC^{total}_{background\ mortality,n}$) included two components: (1) the increment of $CWDC$ induced by background mortality at $year\ n$, and (2) the accumulated $CWDC$ in previous years, of which carbon

losses caused by both consumption (due to stand-replacing fire) and decomposition were accounted for. The calculation of $CWDC^{total}_{background\ mortality,year}$ is described below:

***In 2011*

$$CWDC_{background\ mortality,2011} = AGC_{live,2010} \times (1 - Fraction_{2011}) \times Ratio_{background\ mortality} \quad (15)$$

Thus,

$$CWDC^{total}_{background\ mortality,2011} = CWDC_{background\ mortality,2011} \quad (16)$$

***In 2012*

a. The increment of $CWDC$ induced by background mortality in 2012:

$$CWDC_{background\ mortality,2012} = AGC_{live,2011} \times (1 - Fraction_{2012}) \times Ratio_{background\ mortality} \quad (17)$$

b. $CWDC_{background\ mortality,2011}$ was decayed and consumed in 2012, expressed as:

$$CWDC^{2011}_{background\ mortality,2012} = CWDC_{background\ mortality,2011} \times e^{-k} \times \left(1 - Fraction_{2012} \times Ratio_{CWD_{consumption}}\right) \quad (18)$$

Thus, the total carbon stocks of CWD caused by normal mortality in 2012 was expressed as:

$$CWDC^{total}_{background\ mortality,2012} = CWDC_{background\ mortality,2012} + CWDC^{2011}_{background\ mortality,2012} \quad (19)$$

***In year n:*

The total carbon stocks of CWD ($CWDC^{total}_{background\ mortality,year}$) caused by

normal mortality at $year\ n$ was expressed as:

$$CWDC^{total}_{background\ mortality,n} = CWDC_{background\ mortality,n} + CWDC^{total}_{background\ mortality,n-1} \times e^{-k} \times \left(1 - Fraction_n \times Ratio_{CWD_{consumption}}\right) \quad (20)$$

where $CWDC_{background\ mortality,n}$ was calculated using the following expression:

$$CWDC_{background\ mortality,n} = AGC_{live,n-1} \times (1 - Fraction_n) \times Ratio_{background\ mortality} \quad (21)$$

where $AGC_{live,n-1}$ is AGC_{live} at one year before fire.

Therefore, the total aboveground carbon stocks were expressed as:

***In 2010*

$$AGC_{total,2010} = AGC_{live,2010} + CWD_{initial} \quad (22)$$

***In 2011*

$$AGC_{total,2011} = AGC_{live,2011} + CWD_{initial,2011} + CWDC^{total}_{stand-replacing,2011} + CWDC^{total}_{background\ mortality,2011} \quad (23)$$

**In $year\ n$

$$AGC_{total,n} = AGC_{live,n} + CWD_{initial,n} + CWDC^{total}_{stand-replacing,n} + CWDC^{total}_{background\ mortality,n} \quad (24)$$

Supplementary Figures

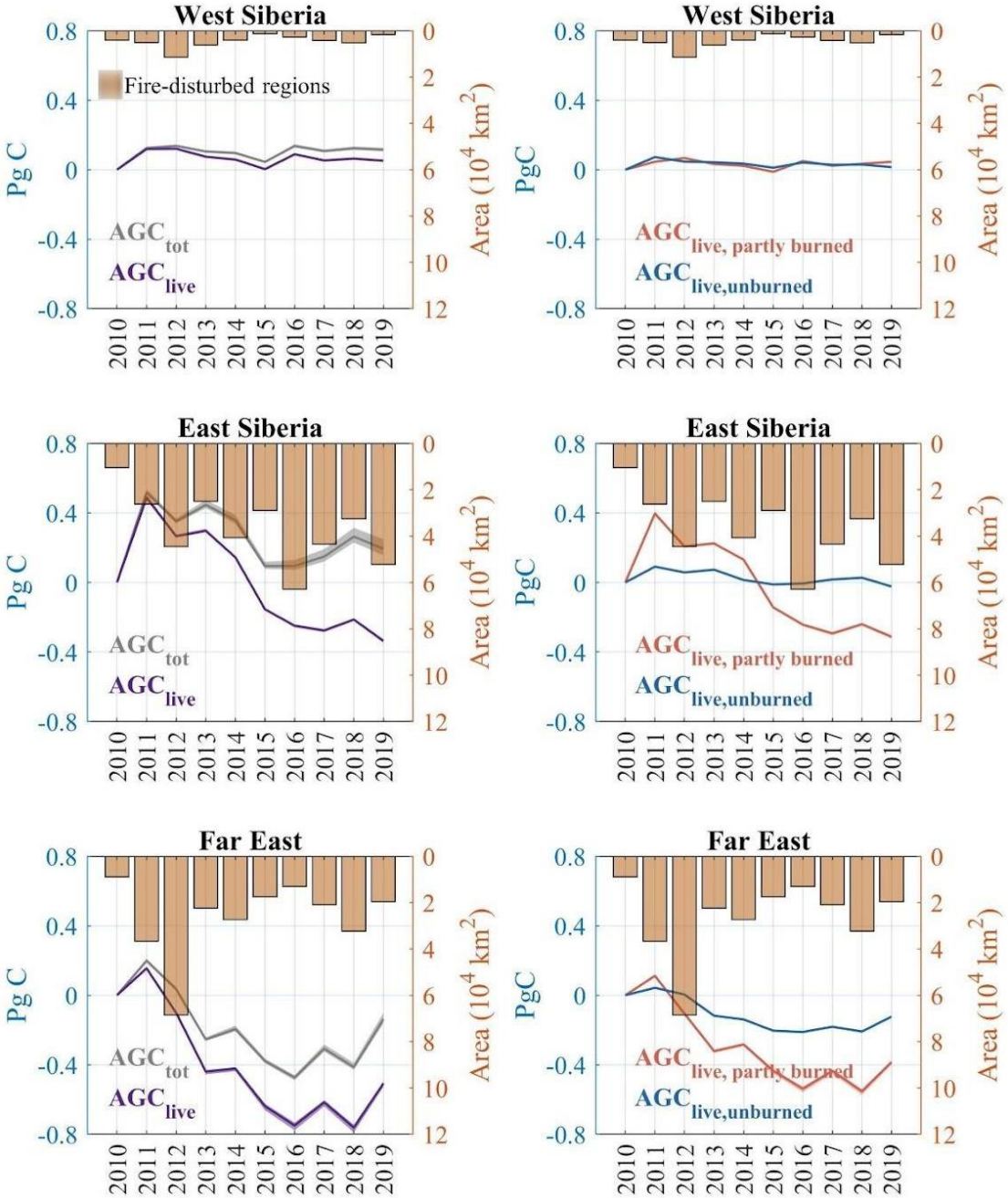

Fig. S1. Temporal variations in annual AGC over the Siberian forests, expressed as the difference from 2010 values. A, C, E, Annual variations in AGC in West Siberia (**A**; n = 817) (49.67° N – 66.14° N, 59.38° E – 89.82° E), East Siberia (**C**; n =

2923) (49.08° N- 67.12° N, 79.09° E- 121.82° E) and Far East regions (**E**; n = 2679) (43.13° N - 69.66° N, 105.74° E - 179.89° E), respectively. **B, D, F,** Corresponding changes in live AGC are shown for partly burned and unburned regions. The ranges represented by shading around the line show the minimum and maximum of AGC changes estimated by six calibrations (Supplementary Table 1). Annual fire-disturbed areas calculated using the MODIS active fire product are indicated by the yellow bar (Method in the main text). Unburned regions were defined as SMOS grids not affected by fire (annual fire area fraction less than or equal to 1% during 2006-2019 and the remaining regions of the Siberia were defined as partly burned regions.

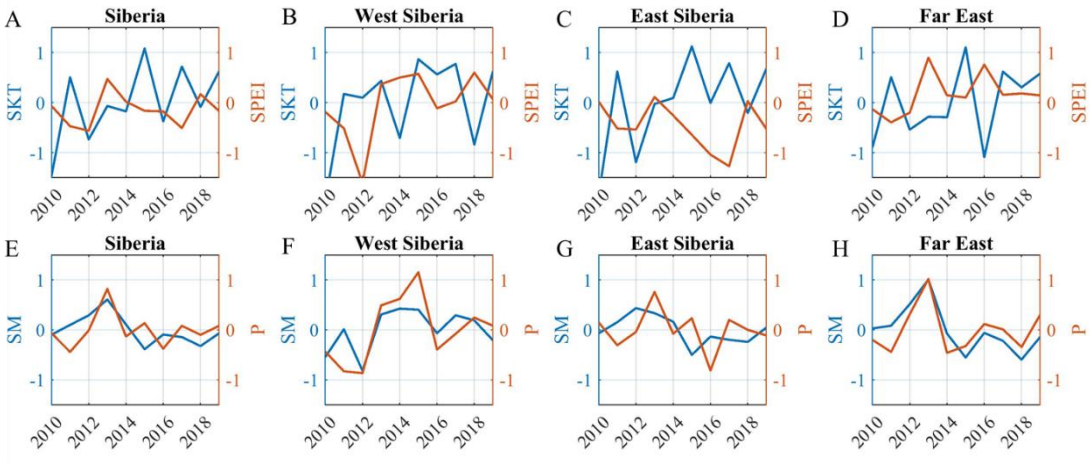

Fig. S2. Anomalies in annual land surface temperature (SKT), the Standardized Precipitation Evapotranspiration Index (SPEI) at 12-month timescale, soil moisture (SM) and precipitation (P). Yearly anomalies were calculated using the z-score: (value − mean)/standard deviation. Precipitation and SKT are provided from ERA5[6].

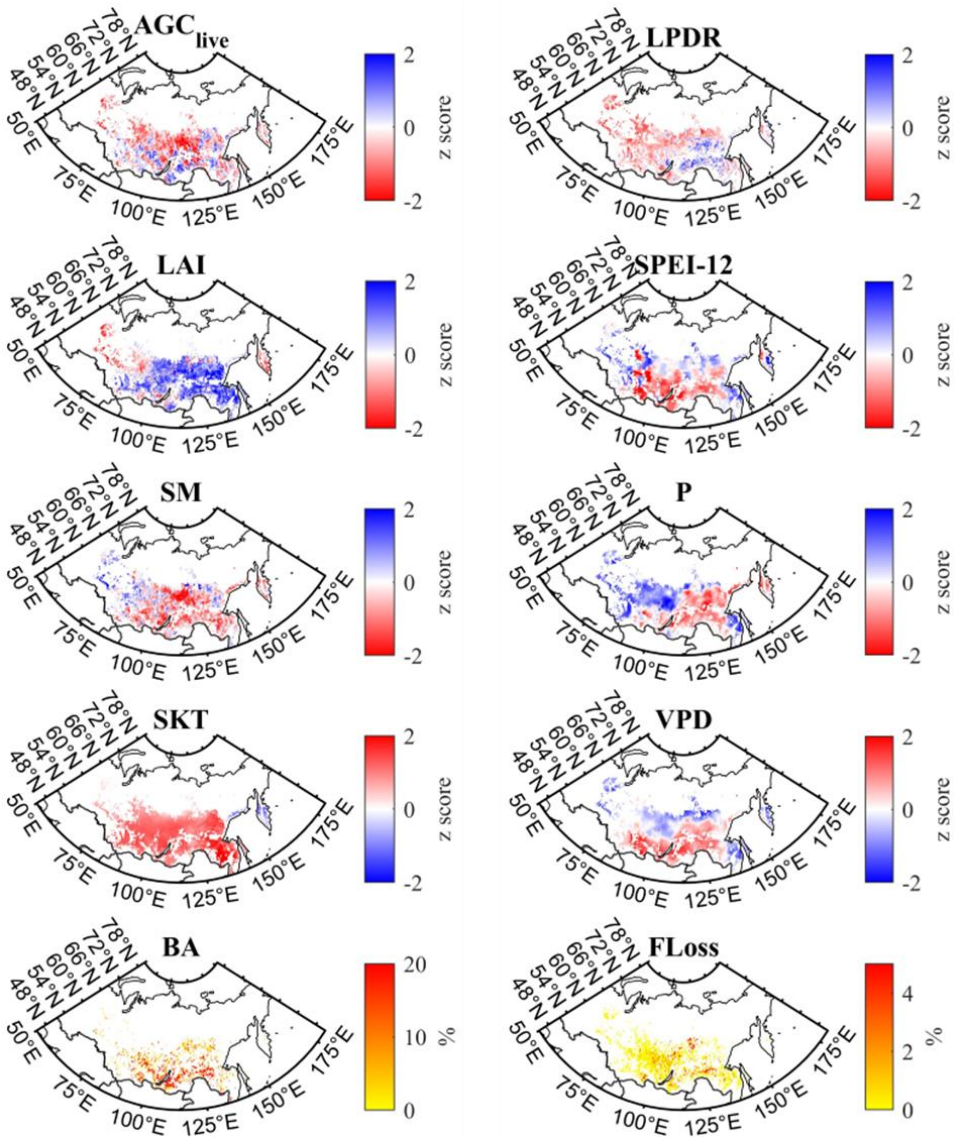

Fig. S3. Spatial patterns of 2015 anomalies in AGC_{live}, LPDR VOD, MODIS growing season LAI, annual SPEI at 12-month timescale, precipitation (P), soil moisture (SM), land surface temperature (SKT), vapour pressure deficit (VPD), annual forest loss (FLoss) and burn area fraction (BA). Yearly anomalies were calculated using the z-score: (value − mean)/standard deviation. Precipitation and SKT are provided from ERA5[6]. VPD was calculated using the method in ref[7] based on the ERA5 dataset.

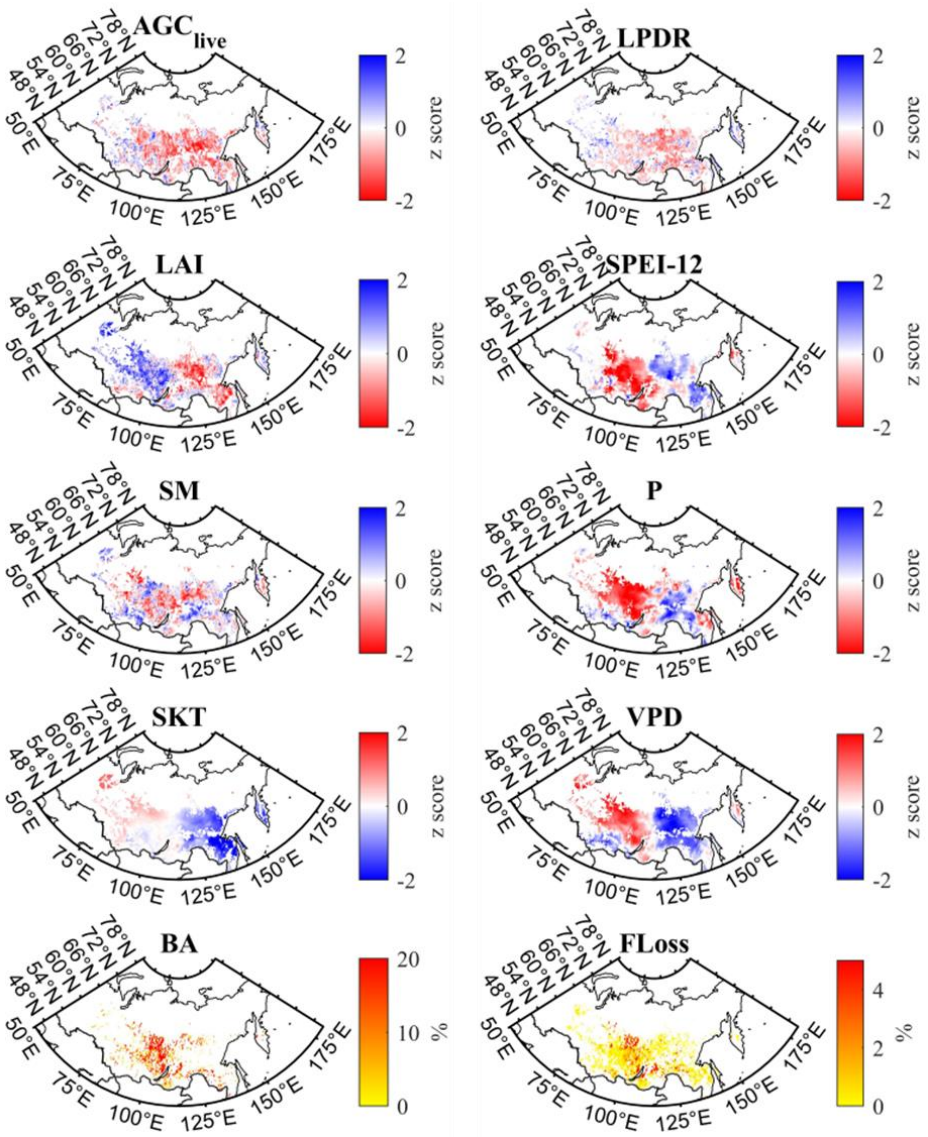

Fig. S4. Same as Fig. S3 but for 2016.

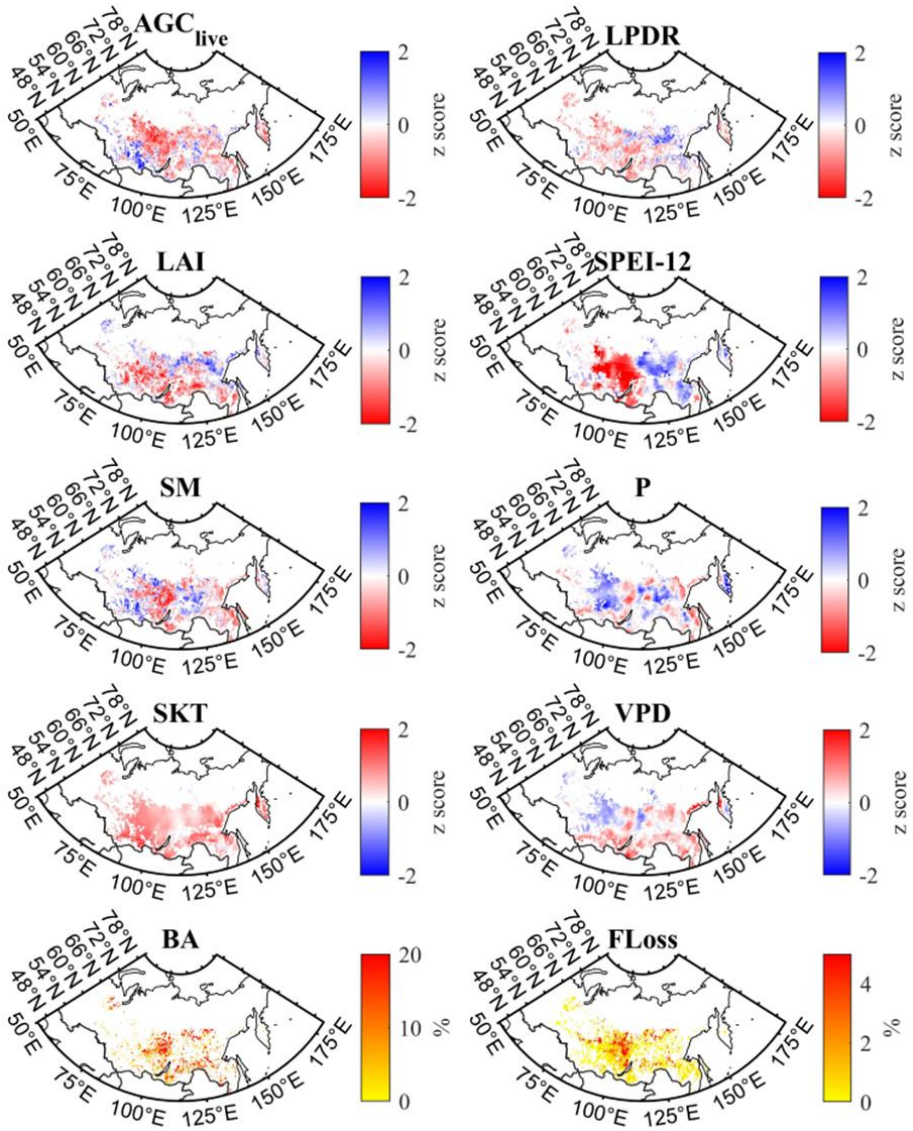

Fig. S5. Same as Fig. S3 but for 2017.

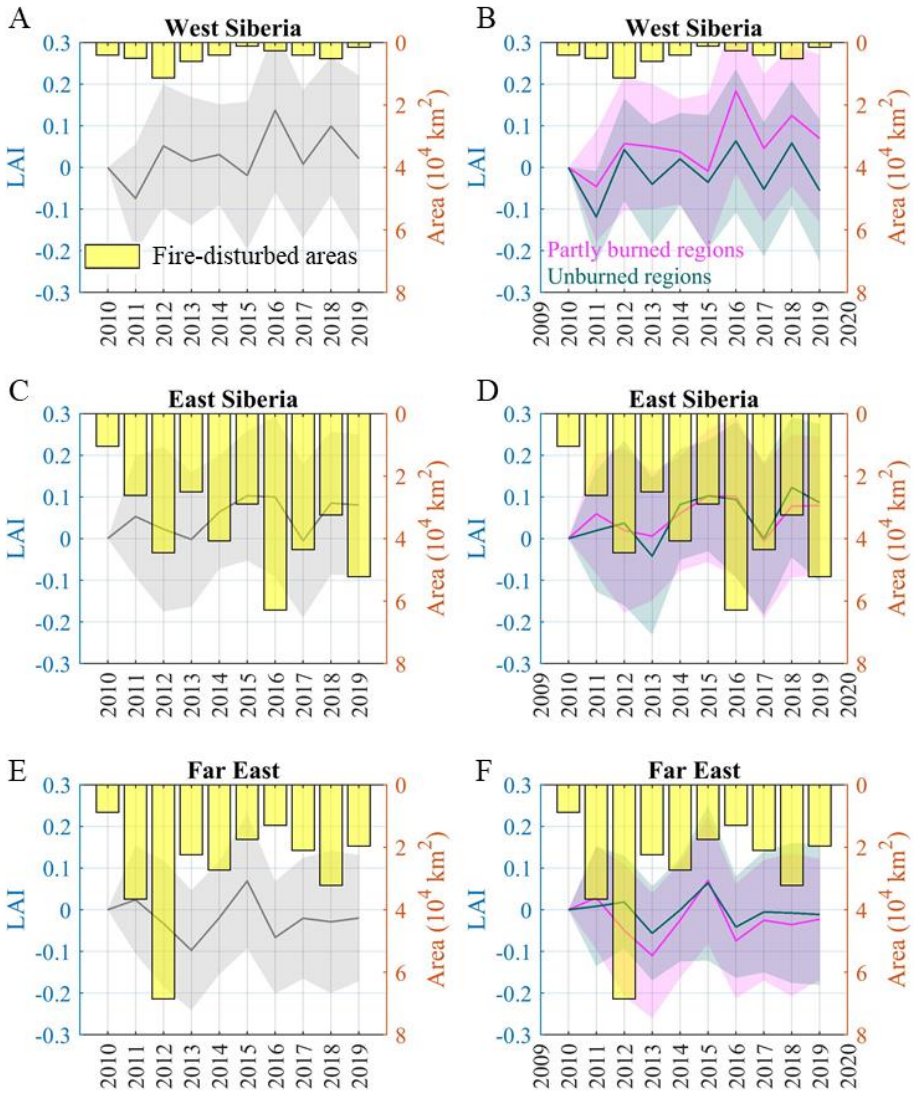

Fig. S6. Same as Fig. S1 but for LAI. The center lines and the shading ranges represent the median values and one standard deviation, respectively.

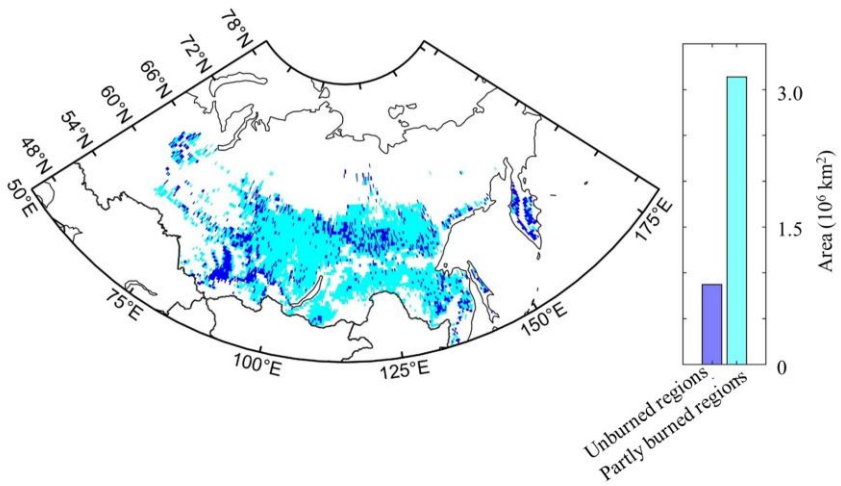

Fig. S7. Unburned and partly burned regions of Siberia. Unburned regions were defined as SMOS grids (~25km) with annual fire area fraction less than or equal to 1% during 2006-2019. Annual active fire areas were estimated by MOD14A2. The remaining regions (annual fire area fraction larger than 1% at least one year of 2006-2019) were defined as partly burned regions.

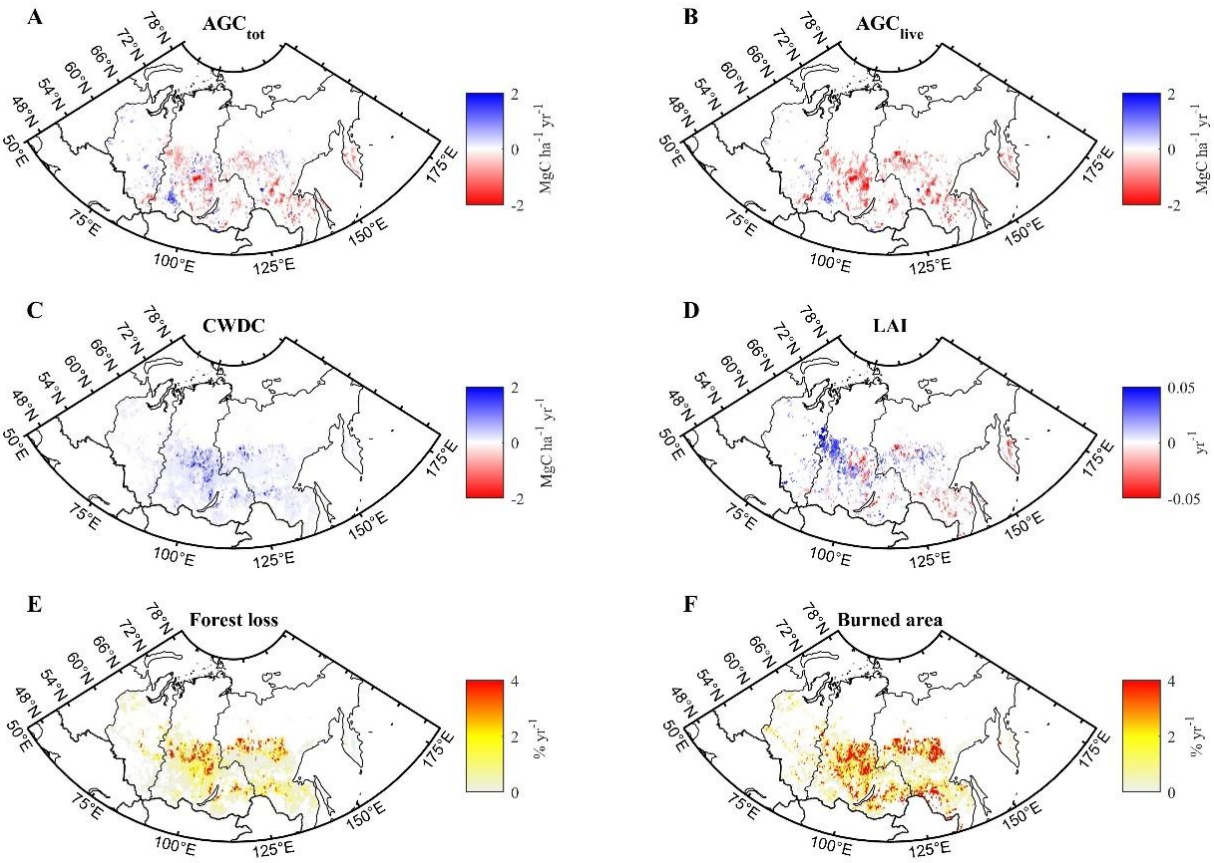

Fig. S8. Spatial patterns of trends in AGC and LAI during 2010-2019. We mapped the significant trends (P<0.05) in AGC_{tot} (**A**), AGC_{live} (**B**), CWDC (**C**) and MODIS LAI (**D**), respectively. Yearly changes in forest-loss (**E**) and burned area (**F**) were estimated using the Hansen and MODIS datasets, respectively, as for Fig. 2E and 2F in the main text. The Theil–Sen test was used to determine trend direction while the Mann–Kendall test was used to assess trends for statistical significance, regarding trends as significant when P < 0.05. (n=6419, 6419, 1750, 2359, 6419, 6419 for **A- F**, respectively)

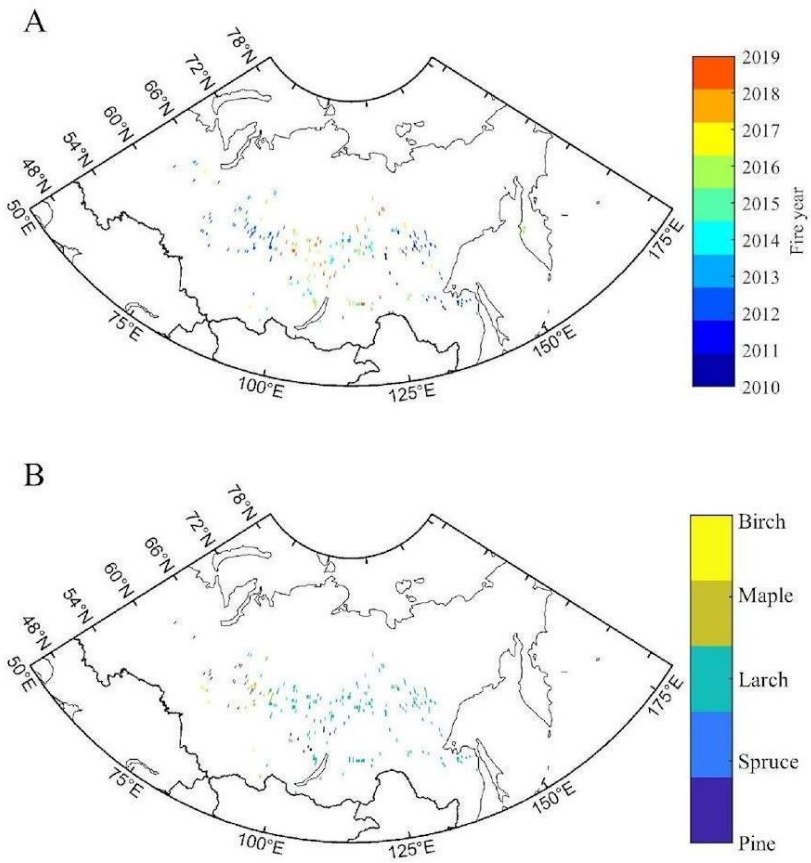

Fig. S9. Fire years and tree species of the selected burned pixels for the calculation of AGC_{live} and LAI loss/recovery in response to wildfires. We selected the burned pixels (n=184) having burned once (less than 1% in the unburned years) during 2006-2019, with the once burned fraction >10% in the burned year (**A**) during 2010-2019. The corresponding tree species, including Birch, Maple, Larch, Spruce and Pine, were mapped (**B**) provided by ref.[8].

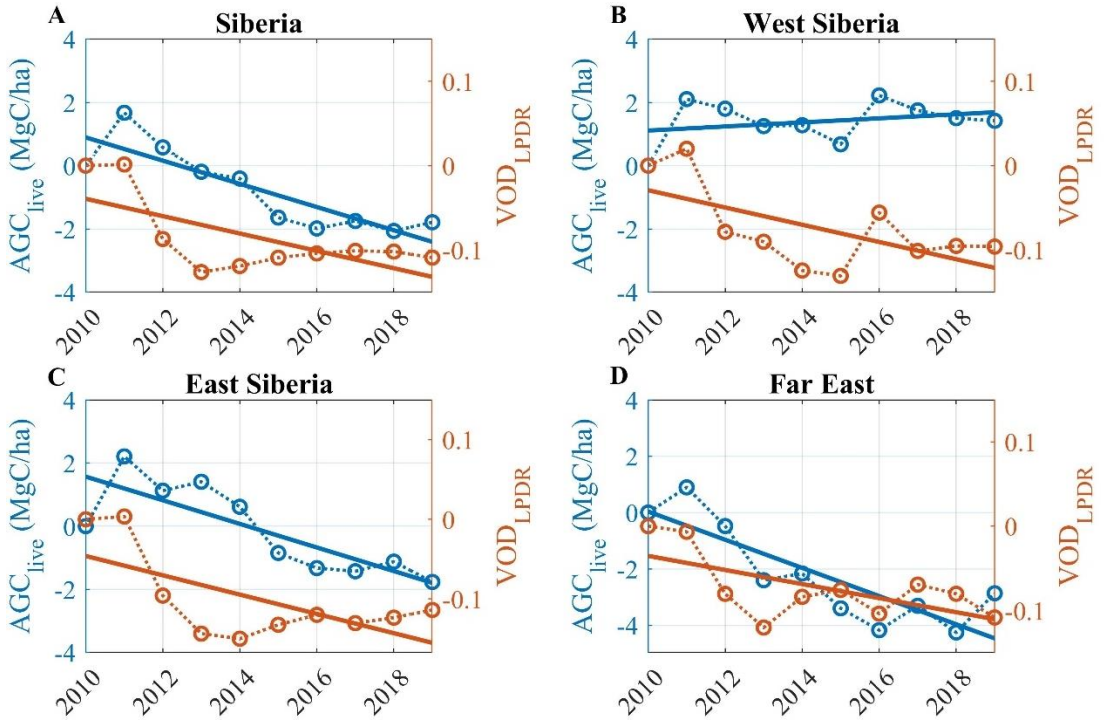

Fig. S10. Time series of AGC_{live} and VOD from LPDR (VOD$_{LPDR}$) during 2010-2019 over the Siberian forests, expressed as the difference from 2010 values. AGC_{live} density was estimated by L-VOD. The Theil–Sen test was used to determine the trend direction and the curves are corresponding linear fitting of the yearly data. Similar interannual variations between AGC_{live} and VOD$_{LPDR}$ can be observed over Siberia and subregions (e.g., West Siberia, East Siberia and Far East).

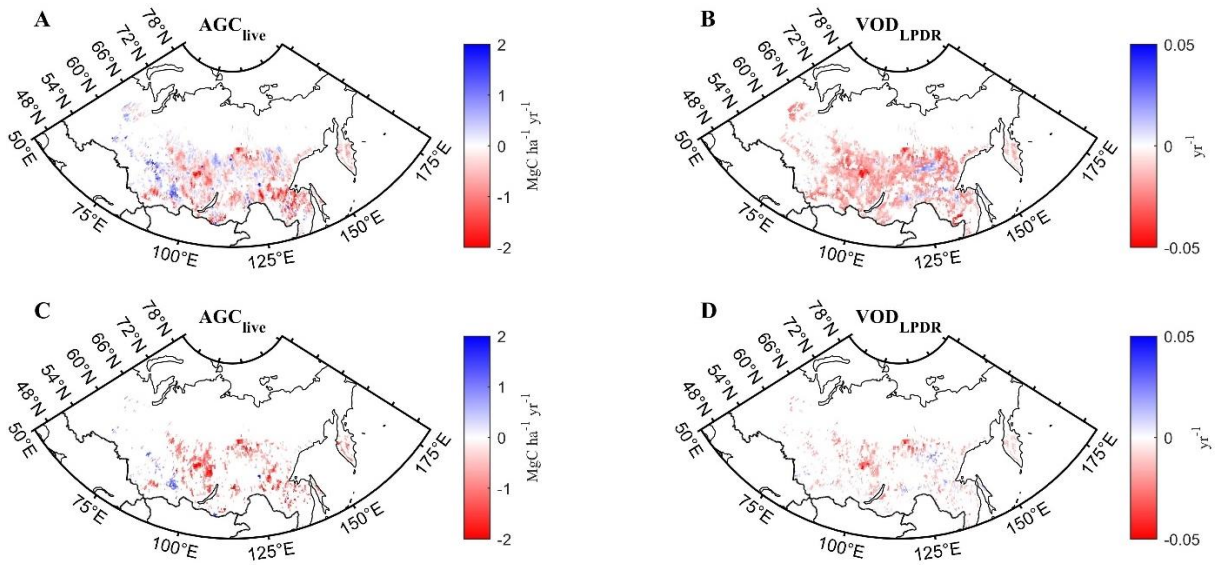

Fig. S11. Spatial patterns of the dynamics (net changes and trends) in AGC_{live} and VOD from LPDR (VOD_{LPDR}) during 2010-2019. We mapped yearly net changes and significant trends (P<0.05) in AGC_{live} (**A, C**), and VOD_{LPDR} (**B, D**), respectively. Theil–Sen test was used to determine trend direction while the Mann–Kendall test was used to assess trends for statistical significance, regarding trends as significant when P < 0.05. L-VOD-derived AGC_{live} and VOD_{LPDR} showed spatially consistent trends: 72% of the pixels showed the same direction of trends (positive or negative) for AGC_{live} and VOD_{LPDR} and 84 % of pixels with net carbon loss matched with negative changes in VOD_{LPDR}.

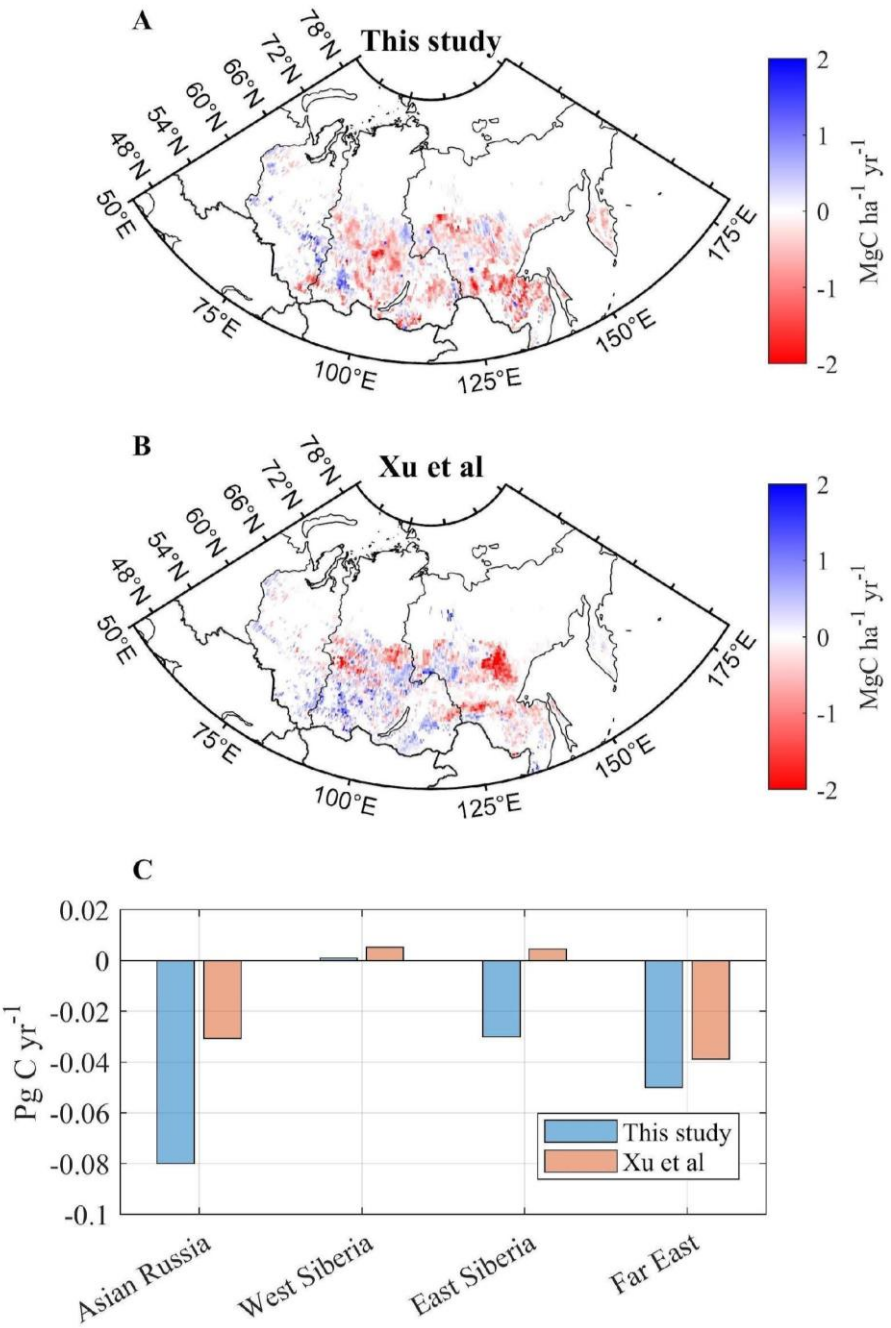

Fig. S12 Comparison between net carbon changes from this study and Xu et al. [9] **between 2010 and 2019.** We mapped net changes in the AGC_{live} from this study **(A)** and the above- and below-ground carbon from Xu et al.[9] **(B)**. The bars **(C)** showed the net carbon changes over Siberia and its subregions (e.g., West Siberia, East Siberia and Far East), estimated from this study and from Xu et al.[9].

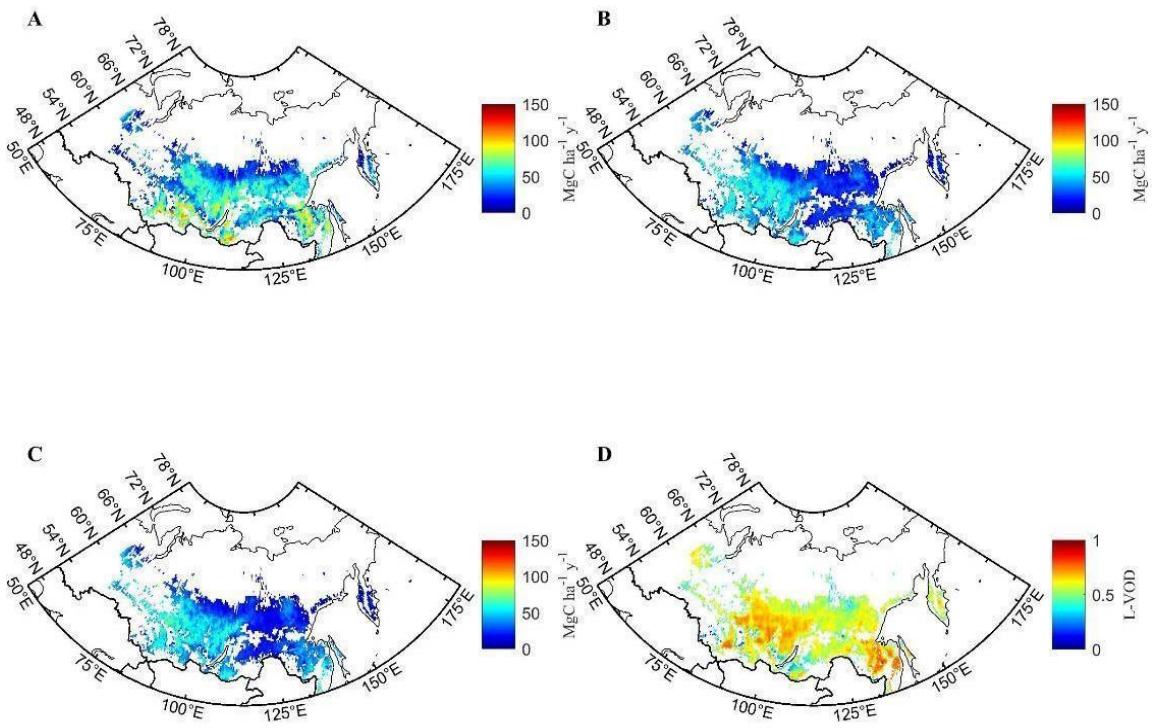

Fig. S13. Maps of the reference AGC_{live} data sets and L-VOD in the Siberia region.

Three reference AGC_{live} density maps are illustrated at a spatial resolution of 25 km: **(A)** Saatchi (Circa 2015), **(B)** CCI (Circa 2017), and **(C)** GlobBiomass (Circa 2010). **(D)** Yearly mean L-VOD in 2011.

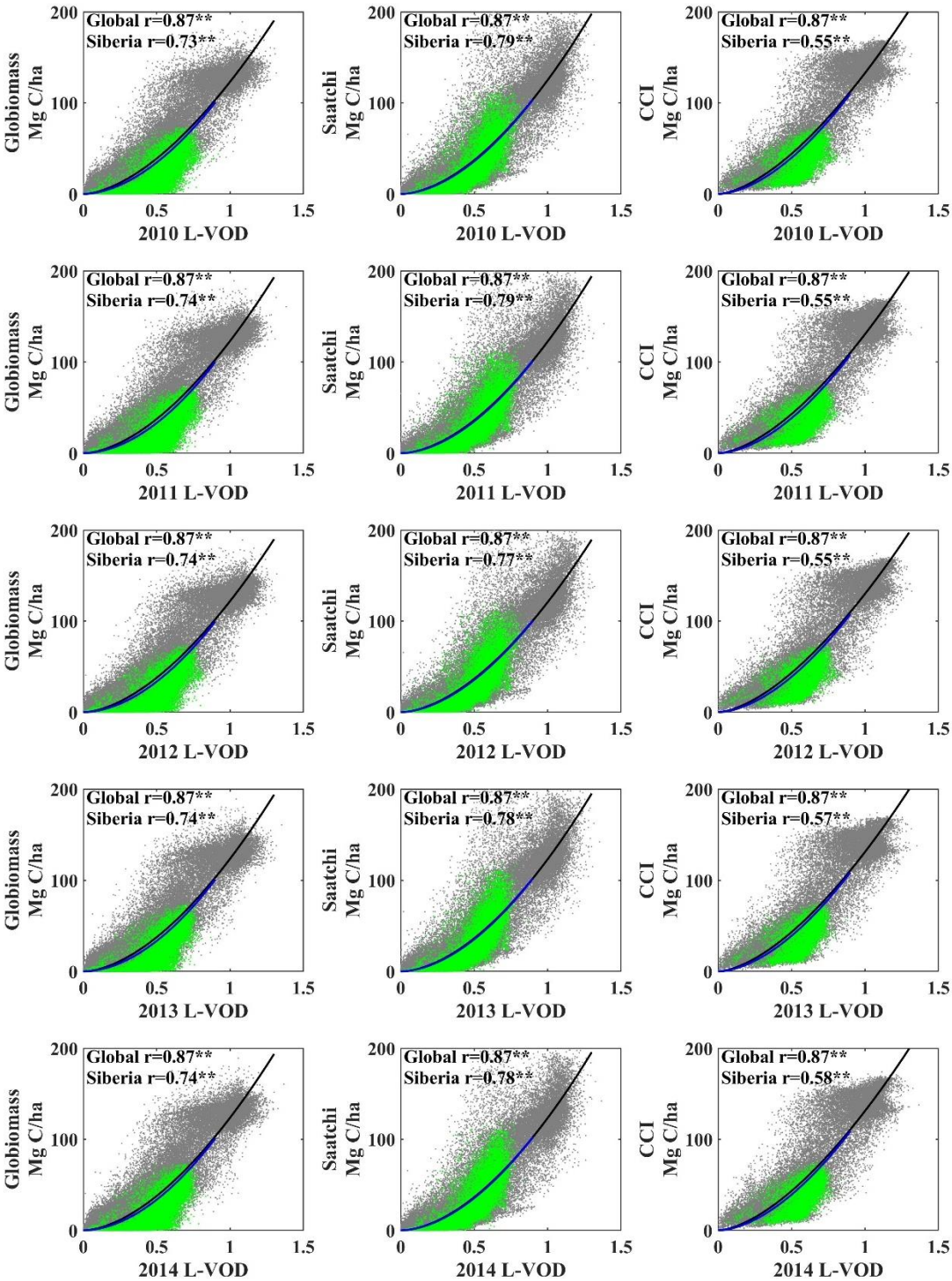

Fig. S14 Relationships between annual L-VOD for different yeas (2010 to 2014) and the benchmark AGC_{live} density (Mg C ha^{-1}) maps at the global scale (referred to as Global) and for Siberia regions. The benchmark AGC_{live} density maps were based on the GlobBiomass (first column), Saatchi (second column) and CCI datasets (third column), respectively. The scatterplots of the Global and Siberia datasets are

indicated in grey and green color, and the corresponding fitted relationships are indicated in black and blue (using Eq.1 in the main text), respectively. The corresponding fitted parameters in 2011 are summarized in Table S1. The results showed that the overall shape of the scatterplots did not change much for different years and the correlation between annual L-VOD and the live AGC benchmark maps were stable.

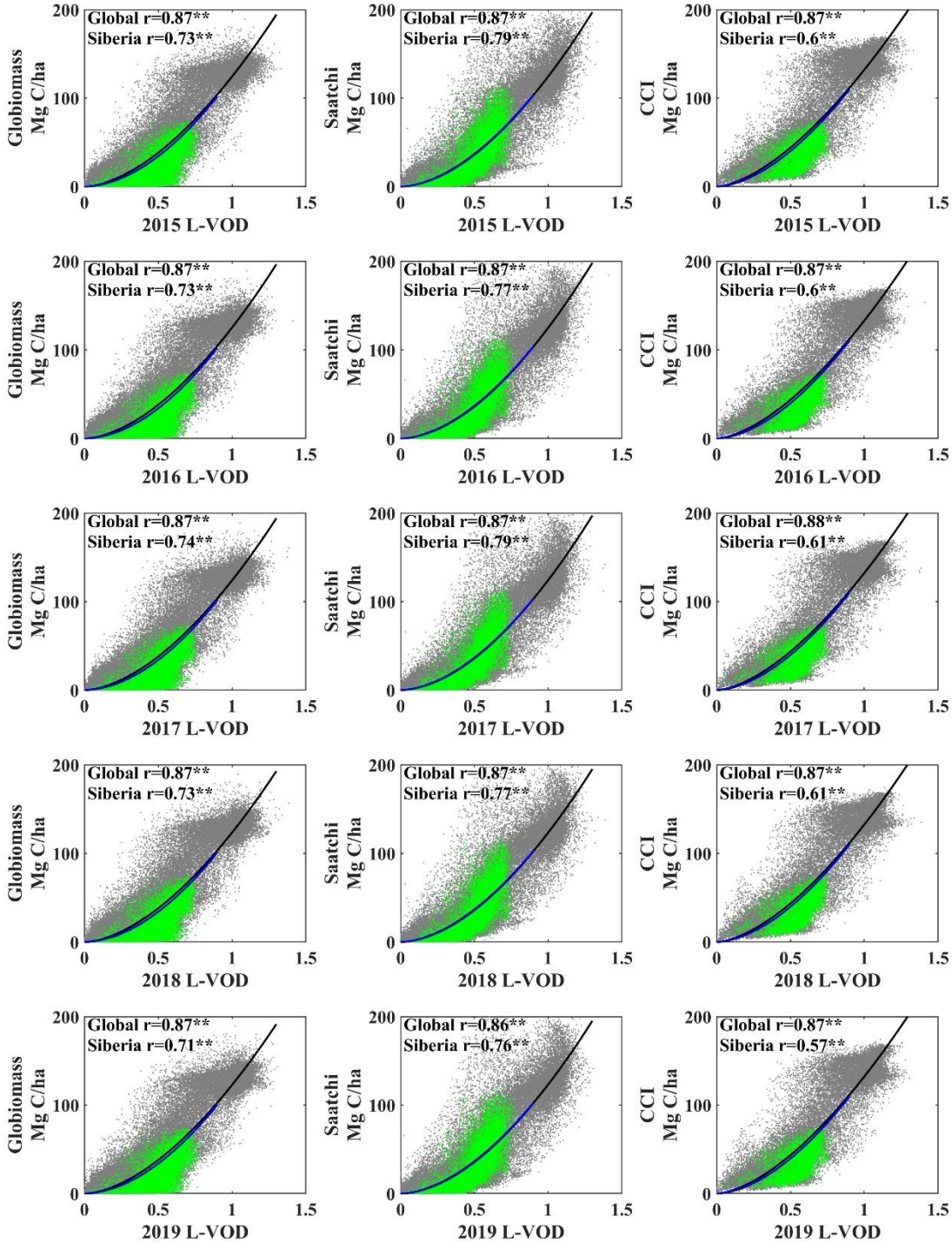

Refer to Fig. S14 (continuation for years 2015 to 2019).

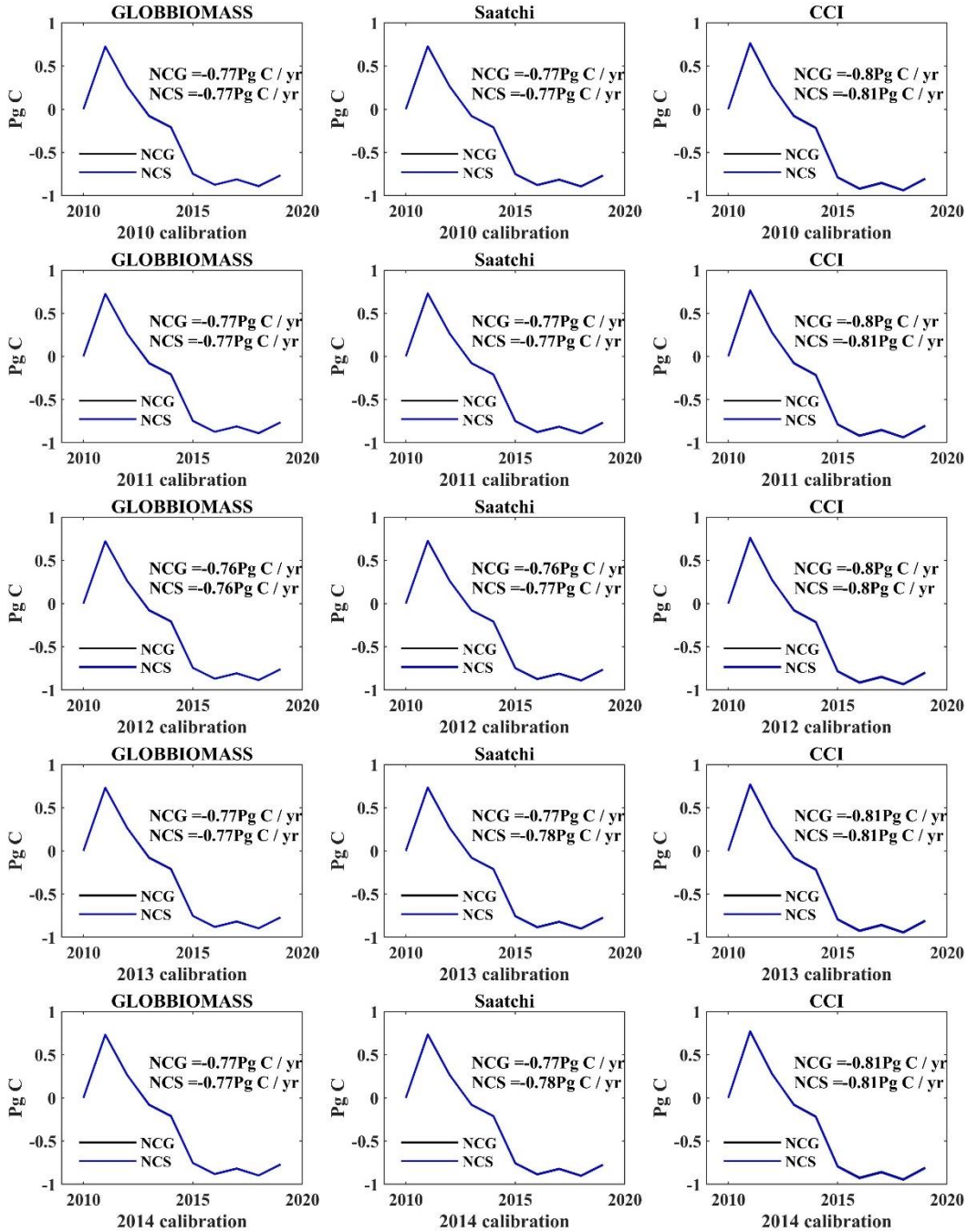

Fig. S15 Live AGC changes over the study region relative to 2010 estimated by the relationship (showed in Fig. S14) calibrated between annual L-VOD for different years (2010 to 2014) and the live AGC benchmark maps. NCG and NCS represented the net live AGC changes over 2010-2019, estimated using the relationship calibrated at the global scale and over Siberia, respectively. The live AGC changes were estimated using the calibrated relationship based on the GlobBiomass (first column), Saatchi

(second column) and CCI benchmark maps (third column), respectively. For example, for the subgraphs in the first column, the Siberia live AGC changes were estimated using the calibrated relationship between GlobBiomass benchmark map and annual L-VOD dataset from different years, respectively.

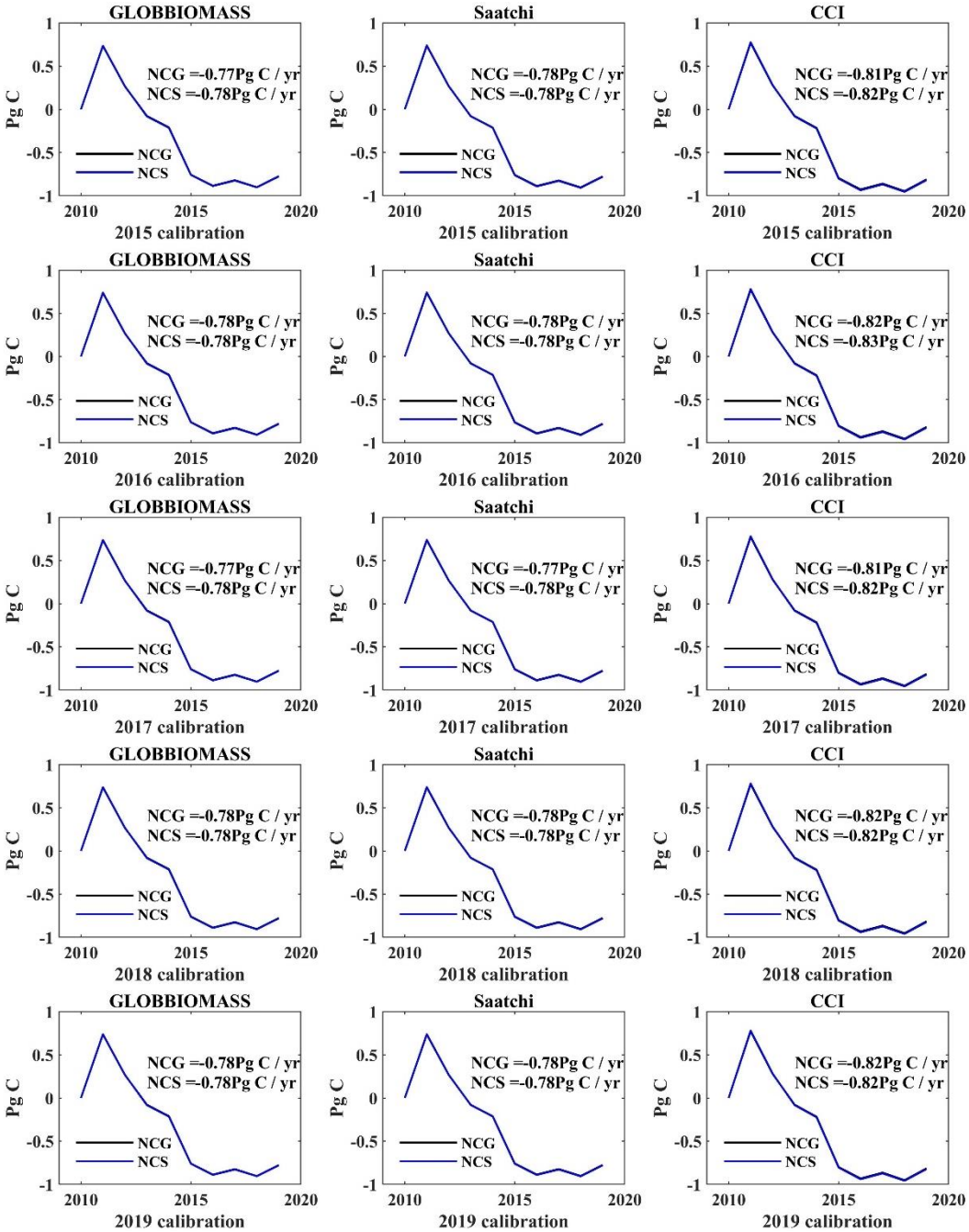

Refer to Fig. S15 (continuation for years 2015 to 2019).

	-1 year	**0 year**	1 year	2 year	3 year	4 year	5 year	6 year	7 year	8 year	9 year
Pixel 1		2010	2011	2012	2013	2014	2015	2016	2017	2018	2019
Pixel 2	2010	2011	2012	2013	2014	2015	2016	2017	2018	2019	
Pixel 3	2011	2012	2013	2014	2015	2016	2017	2018	2019		
Pixel 4	2012	2013	2014	2015	2016	2017	2018	2019			
Pixel 5	2014	2015	2016	2017	2018	2019					
Pixel 6	2015	2016	2017	2018	2019						
Pixel 7	2016	2017	2018	2019							
Pixel 8	2017	2018	2019								
Pixel 9	2018	2019									

Fig. S16 Example showing how the 10-year time series was built for the AGC_{live}/LAI recovery. Zero on the time scale of the time series represents the year of burn. The years in the grey columns show the timing of burn.

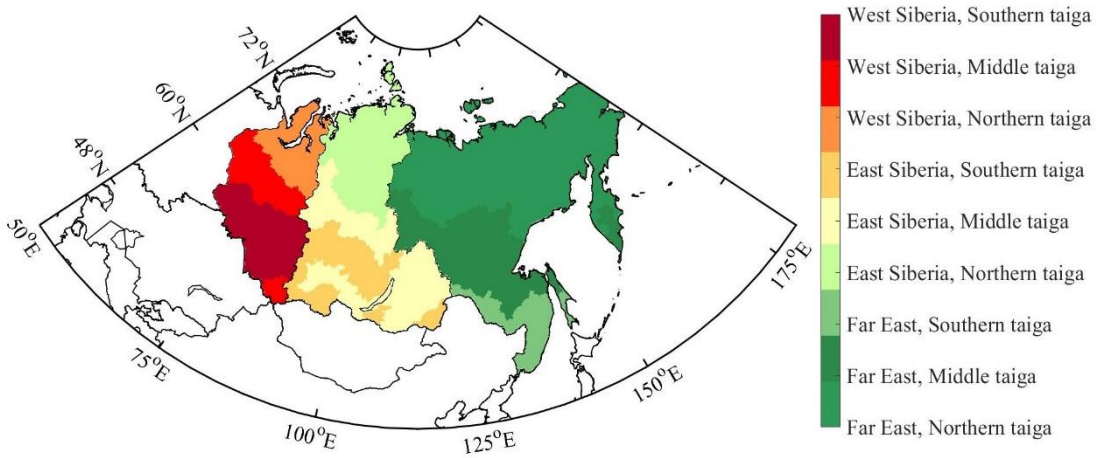

Fig. S17 Distribution of the three geographic regions (West Siberia, East Siberia and Far Ease) and the three bioclimatic zones (North, Middle and South Taiga)[10] **considered in the present study.**

Supplementary Tables

Table S1. Parameters of the exponential function ($AGC_{live} = a \times VOD^{b}$) used to fit the spatial relationship between the benchmark live AGC and L-VOD in Fig. S14. Values are given for the three benchmark maps for two areas (Siberia and at the global scales)

Abbreviation	Benchmark live AGC maps	Region	*a*	*B*	*r*
$P_{Global\ Globbiomass}$	Globbiomass	Global	123.118	1.713	0.87**
$P_{Siberia\ Globbiomass}$	Globbiomass	Siberia	122.048	1.879	0.74**
$P_{Global\ Saatchi}$	Saatchi	Global	122.464	1.756	0.87**
$P_{Siberia\ Saatchi}$	Saatchi	Siberia	122.549	1.811	0.79**
$P_{Global\ CCI}$	CCI	Global	130.572	1.603	0.87**
$P_{Siberia\ CCI}$	CCI	Siberia	129.590	1.7501	0.55**

** indicates significant correlations at $P < 0.01$.

Table S2. Comparison of the reference live AGC and retrieved live AGC data in 2011 using six sets of parameters ($P_{Global\ Saatchi}$, $P_{Siberia\ Saatchi,\ ...,}$ $P_{Siberia\ Globbiomass}$) for the same spatial extent over global and Siberia regions (the spatial extent corresponds to the one used for the calibration of the reference L-VOD / live AGC relationships). The bootstrap cross-validated RMSE of the retrieved live AGC stocks is shown in parentheses. The 95% bootstrap confidence interval is shown in square brackets. Correlation values (r) of the spatial correlation between the reference live AGC density and the corresponding bootstrap live AGC density estimates are given in the right side of the table. The computation of the uncertainties includes only internal errors associated with each reference biomass map.

	Global (Pg C)	Siberia (Pg C)	r
Reference live AGC maps			
Saatchi map	189.6	19.4	
CCI map	208.8	13.8	
Globbiomass map	198.0	14.0	
L-VOD-retrieved AGC_{live}			
AGC_{live} *retrieved using* $P_{Global\ Saatchi}$	189.7 (4.0) [189.0, 190.3]		0.92**
AGC_{live} *retrieved using* $P_{Siberia\ Saatchi}$		19.4 (0.3) [19.3, 19.6]	0.95**
AGC_{live} *retrieved using* $P_{Global\ CCI}$	208.8 (3.3) [208.1, 209.4]		0.93**
AGC_{live} *retrieved using* $P_{Siberia\ CCI}$		13.8 (0.4) [13.7, 13.9]	0.88**
AGC_{live} *retrieved using* $P_{Global\ Globbiomass}$	197.9 (2.8) [197.4, 198.5]		0.92**
AGC_{live} *retrieved using* $P_{Siberia\ Globbiomass}$		14.0 (0.4) [13.8, 14.1]	0.91**

*/** indicate significant correlations at $P < 0.05/0.01$.

Table S3. The decomposition rate (k, in unit of yr $^{-1}$) based on plot-level studies. The k values over each regionwere calculated as the weighted average k value for each subregion based on the k value for separate tree species and their contributions over the corresponding region[11-14].

Regions	Western Siberia	East Siberia	Far East
Northern taiga	0.022	0.014	0.009
Middle taiga	0.029	0.031	0.019
Southern taiga	0.037	0.035	0.034

Table S4. Coarse woody debris carbon to AGC_{live} ratio at the initial year of 2010 ($Ratio_{initial}$)[11,13,15,16]. The average value of all $Ratio_{initial}$ values over each region was calculated as the $Ratio_{initial}$ value of the corresponding region.

Regions	Western Siberia	East Siberia	Far East
Northern taiga	0.26	0.23	0.24
Middle taiga	0.26	0.29	0.28
Southern taiga	0.21	0.27	0.26

Table S5. Ratio of the AGC_{live} consumption to AGC_{live} during stand-replacing fire event ($Ratio_{AGC_{consumption}}$)[16]. The average value of all $Ratio_{AGC_{consumption}}$ values over each region was calculated as the $Ratio_{AGC_{consumption}}$ value of the corresponding region.

Regions	Western Siberia	East Siberia	Far East
Northern taiga	0.082	0.081	0.087
Middle taiga	0.085	0.076	0.090
Southern taiga	0.079	0.077	0.101

Table S6. Ratio of $CWDC$ consumption to $CWDC$ during stand-replacing fire event ($Ratio_{CWD_{consumption}}$)[17,18]. The average value of all $Ratio_{CWD_{consumption}}$ values over each region was calculated as the $Ratio_{CWD_{consumption}}$ value of the corresponding region.

Regions	Western Siberia	East Siberia	Far East
Northern taiga	0.59	0.50	0.54
Middle taiga	0.63	0.63	0.60
Southern taiga	0.64	0.64	0.64

Table S7. Ratio of natural annual wood mortality to AGC_{live} ($Ratio_{background\ mortality}$)[19]. The average value of all $Ratio_{background\ mortality}$ values over each region was calculated as the $Ratio_{background\ mortality}$ value of the corresponding region.

Regions	Western Siberia	East Siberia	Far East
Northern taiga	0.0067	0.0092	0.0194
Middle taiga	0.0093	0.0072	0.0089
Southern taiga	0.0131	0.0110	0.0114

Reference in the Supplementary Information

1. Shvidenko, A. & Schepaschenko, D. Climate change and wildfires in Russia. *Contemporary Problems of Ecology.* **6**, 683-692 (2013).
2. Harmon, M. E. *et al.* Release of coarse woody detritus-related carbon: a synthesis across forest biomes. *Carbon balance and management.* **15**, 1-21 (2020).
3. Bartalev, S. A. & Stytsenko, F. V. Assessment of Forest-Stand Destruction by Fires Based on Remote-Sensing Data on the Seasonal Distribution of Burned Areas. *Contemporary Problems of Ecology.* **14**, 711-716 (2021).
4. Curtis, P. G. *et al.* Classifying drivers of global forest loss. *Science.* **361**, 1108-1111 (2018).
5. van Wees, D. *et al.* The role of fire in global forest loss dynamics. *Global Change Biology.* **27**, 2377-2391 (2021).
6. Hersbach, H. *et al.* The ERA5 global reanalysis. *Quarterly Journal of the Royal Meteorological Society.* **146**, 1999-2049 (2020).
7. Yuan, W. *et al.* Increased atmospheric vapor pressure deficit reduces global vegetation growth. *Science Advances.* **5**, eaax1396 (2019).
8. Schepaschenko, D. *et al.* A new hybrid land cover dataset for Russia: a methodology for integrating statistics, remote sensing and in situ information. *Journal of Land Use Science.* **6**, 245-259 (2011).
9. Xu, L. *et al.* Changes in global terrestrial live biomass over the 21st century. *Science Advances.* **7**, eabe9829 (2021).
10. Loboda, T. V. & Chen, D. Spatial distribution of young forests and carbon fluxes within recent disturbances in Russia. *Global change biology.* **23**, 138-153 (2017).
11. Ivanov, A. V. *et al.* Large Wooden Debris' Contribution into a Biogenic Carbon Cycle in Coniferous-Deciduous Forests of the Southern Regions of Russian Far East. *Lesovedenie (Russian Journal of Forest Science).* **4,** 357-366 (2020).[in Russian].
12. Mukhin, V. A. & Voronin, P. Y. Mycogenic decomposition of wood and carbon emission in forest ecosystems. *Russian Journal of Ecology.* **38**, 22-26 (2007).
13. Vedrova, E. F. *et al.* Contribution of Old Growth Forests to the Carbon Budget of the Boreal Zone in Central Siberia. *Biology Bulletin.* **45**, 288-297 (2018).
14. Zamolodchikov, D. G. *et al.* Carbon Pools and Fluxes in Forests of Far East Federal Region. *Coniferous of the boreal zone.* **23**, 21-30 (2006).[in Russian].
15. Malysheva, N. *et al.* Assessment of coarse woody debris stock in Russian forests based on state forest inventory data. *IOP Conference Series: Earth and Environmental Science.* **316**, 012033 (2019).
16. Shvidenko, A. *et al.* Coarse wood detritus pool in Russian forests. *Forest mensuration and forest management.* **1**, 133-147 (2009).[in Russian].
17. Shvidenko, A. *et al.* Impact of wildfire in Russia between 1998–2010 on ecosystems and the global carbon budget. *Doklady Earth Sciences.* **441**, 1678-1682 (2012).
18. Zhila, S. V. Transformation of Phytomass in Light-Coniferous Plantations of the Lower Angara Region Under the Influence of Fires. *PhD thesis.*

Krasnoyarsk. (2013).[in Russian].
19. Shvidenko, A. *et al.* Tables and models of growth and productivity of forests of major forest forming species of Northern Eurasian. *Moscow: Federal Agency of Forest Management of the Russian Federation and International Institute for Applied Systems Analysis.* (2008).[in Russian].